

## Test Particle Transport due to Long Range Interactions

F. Anderegg, X.-P. Huang,\* C. F. Driscoll, E. M. Hollmann, T. M. O'Neil, and D. H. E. Dubin

*Institute for Pure and Applied Physical Sciences and Department of Physics, University of California at San Diego,  
La Jolla, California 92093*

(Received 31 October 1996)

Enhanced cross-field transport of test particles is observed in a quiescent, steady-state pure ion plasma. The measured particle diffusion is about ten times faster than predicted by classical collisional theory over a wide range of densities, temperatures, and magnetic fields, whereas the measured velocity-space isotropization agrees closely with collisional theory. This enhanced diffusion scales essentially as  $B^{-2}$  and is probably due to long-range “ $\mathbf{E} \times \mathbf{B}$  drift” collisions, with interaction distances  $\rho$  in the range  $r_c < \rho < \lambda_D$ . [S0031-9007(97)02594-5]

PACS numbers: 52.25.Fi, 52.25.Wz

Collisional transport of particles and energy across magnetic field lines is an active area of plasma theory and experiments, with fundamental questions as to the binary vs collective and short-range vs long-range nature of interparticle collisions. Classical Boltzmann theory [1] describes ion transport in terms of local collisions, with impact parameters less than the cyclotron radius, i.e.,  $\rho \leq r_c$ ; but it has long been recognized that electron particle and heat transport may involve long-range collisions, with  $r_{ce} < \rho \leq \lambda_D$  [2,3]. In  $Q$  machines, experiments with optical tagging of ions [4] have demonstrated classical collisional diffusion [5,6] and shear-induced convection [7]. In fusion plasmas, tritium diffusion and convection coefficients have been obtained from neutron emission, but direct comparison to theory is still ambiguous [8]. Measurements of bulk transport in pure electron plasma have shown enhanced viscosity thought to be due to long-range interactions [9]; and the present experiments are an attempt to quantify these interactions.

Here, we measure cross-field test-particle transport in an unneutralized ion plasma, where the cyclotron radius is smaller than the Debye length, i.e.,  $r_c < \lambda_D$ . The quiescent, near-thermal-equilibrium ion column is contained steady state in a Penning-Malmberg trap [10], with no net transport or particle loss. Ions are tagged by spin orientation, and the slow cross-field diffusion of these test particles is accurately measured using laser-induced fluorescence (LIF).

This test particle diffusion has been measured over a wide range of density, temperature, and magnetic field, and is generally about ten times faster than predicted by the classical theory of velocity-scattering collisions. Measurements of velocity-space isotropization on the same ion plasmas agree closely with classical theory [11,12], indicating there is no uncertainty in this collision rate. The enhanced test particle diffusion scales essentially as  $B^{-2}$ , and is probably due to long-range “ $\mathbf{E} \times \mathbf{B}$  drift” collisions with  $r_c < \rho < \lambda_D$  [2,3]. These weak, long-range binary interactions between ions are ultimately limited by velocity-scattering collisions and by shear in the  $\mathbf{E} \times \mathbf{B}$  rotation of the column.

Figure 1 shows the cylindrical trap and confined pure ion plasma, with parallel and perpendicular laser beams and LIF detection [13]. The electrodes are of radius  $R_w = 2.86$  cm, and are contained in a vacuum chamber with  $P = 3 \times 10^{-9}$  Torr (97%  $\text{H}_2$ ). Magnesium ions are obtained from a brief discharge of the metal vapor vacuum arc source [14]. The ions are trapped by positive voltages applied to the end cylinders, whereas free electrons are ejected axially. Basic radial confinement is provided by a uniform axial magnetic field  $0.8 < B < 4$  T, which by itself would result in plasma loss times from neutral collisions and static field asymmetries [15] of  $\tau_L \leq 2000$  s. The loss time is made essentially “infinite” ( $> 2$  weeks) by applying weak “rotating wall” potentials ( $\leq 1V_{pp}$ ) to eight azimuthal wall sectors. This rotating field, varying as  $e^{im\theta - i\omega t}$ , with  $m = 1$ , adds angular momentum and energy to the plasma, balancing the background drag and energy losses.

LIF measurements use a 280 nm laser beam ( $\sim 1$  mW, bandwidth 1 MHz) produced by a frequency-doubled tunable continuous (CW) ring dye laser using a nonlinear crystal in an externally stabilized optical cavity [16]. At each radial position, the frequency of the laser is swept 60 GHz through a  $3^2S_{1/2} \rightarrow 3^2P_{3/2}$  “cyclone”

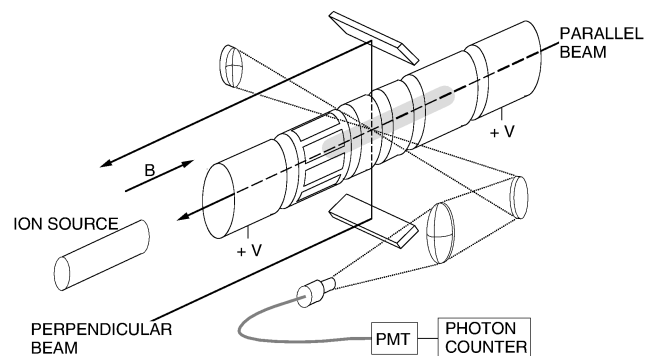


FIG. 1. Schematic diagram of the cylindrical ion trap, with perpendicular and parallel laser beams and LIF detector. A “rotating wall” drive applied to the segmented electrode gives steady-state confinement.

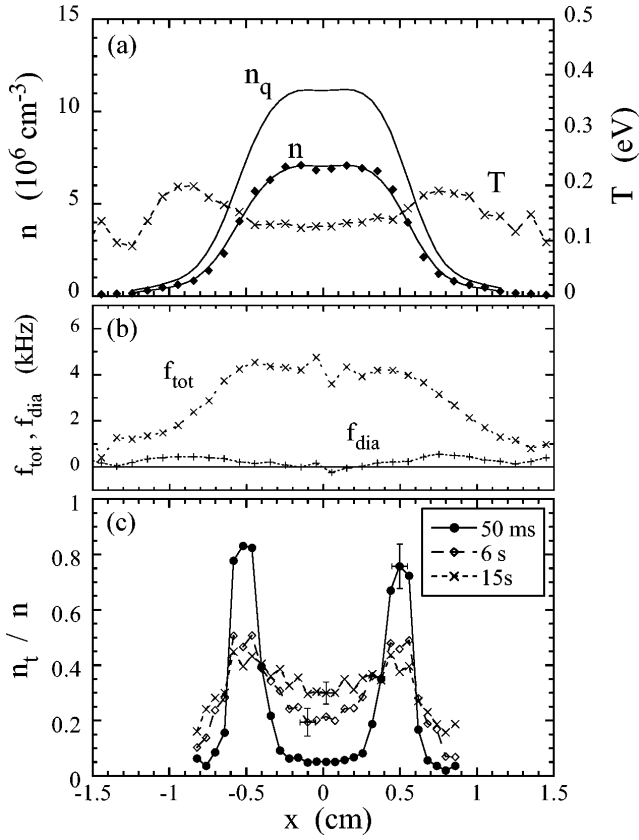


FIG. 2. (a) Measured  $\text{Mg}^+$  density  $n(r)$  and temperature  $T(r)$ , with inferred total charge density  $n_q(r)$ . (b) Measured fluid rotation rate  $f_{\text{tot}}(r)$  and calculated diamagnetic rotation rate  $f_{\text{dia}}$ . (c) Measured test particle density  $n_t(r,t)/n(r)$  at three times, showing radial diffusion towards  $n_t/n = \text{const}$ .

transition of  $\text{Mg}^+$  in 1.7 s, to obtain the  $\theta$ -averaged ion velocity distribution. Figures 2(a) and 2(b) show density, temperature, and rotation profiles for an ion plasma that has been confined for 27 hours with  $B = 4 \text{ T}$ . LIF measurements give  $\text{Mg}^+$  density  $n(r)$ , temperature  $T(r)$ , and total velocity azimuthal drift  $v_{\text{tot}}(r) \equiv 2\pi r f_{\text{tot}}(r)$ .

We estimate the total confined charge density as  $n_q(r) = \alpha n(r)$ , with  $\alpha$  obtained from a fit to  $v_{\text{tot}}(r) = (c/B) [E(r) - \nabla(nT)/ne]$  with  $\nabla E(r) = 4\pi e n_q(r)$ . For this plasma, about 65% of the charge is  $\text{Mg}^+$ , with  $\text{MgH}_n^+$  probably constituting most of the remainder. For  $T > 0.01 \text{ eV}$  no mass separation is observed, and  $\text{MgH}_n^+$  has the same spatial distribution as  $\text{Mg}^+$  [17]. The ion plasma has axial length  $L_p \approx 10 \text{ cm}$ , and individual ions bounce axially at a rate  $f_b \equiv \bar{v}/2L_p \approx 3 \text{ kHz}$  for average thermal energy  $T = 0.1 \text{ eV}$ .

The ion plasma tends to cool to about 0.05 eV due to collisions with neutrals. We control the temperature either by ion cyclotron resonance heating from an  $m = 1$  voltage applied to wall sectors, or by compressional heating from an  $m = 0$  voltage applied to an end cylinder. Both techniques were used in the data presented here, with no noticeable differences in the resulting test particle transport.

The  $M_j = \pm \frac{1}{2}$  spin orientation of the  $3^2S_{1/2}$  ground state of  $\text{Mg}^+$  is used to “tag” the test particles [18]. These parallel/antiparallel orientations have negligible energy difference ( $4.6 \times 10^{-4} \text{ eV}$  at 4 T), so the system eventually relaxes to equal populations. However, measurements establish that the spin orientation of an ion is relatively robust, degrading with a time constant  $10^4 \text{ s} > \tau_s > 10 \text{ s}$  for  $0.05 \leq T \leq 5 \text{ eV}$ . This is longer than the time required for the tagged ions to diffuse radially.

Three steps are used to measure test particle transport.

(A) Reset. The plasma is completely ( $>98\%$ ) polarized into the  $S_{1/2}^{M_j=-1/2}$  state by direct optical pumping with a beam tuned to  $S_{1/2}^{M_j=+1/2} \rightarrow P_{3/2}^{M_j=-1/2}$  transition. This beam is perpendicular to the magnetic field and passes through the center of the plasma.

(B) Tag. The spin of particles at a chosen radial position  $r_t$  is reversed by direct optical pumping with a parallel beam tuned to  $S_{1/2}^{M_j=-1/2} \rightarrow P_{3/2}^{M_j=+1/2}$ . The tagging beam is left on for many rotations of the plasma and also for many bounce periods to ensure that most ions are pumped; typically 50 ms are required to locally tag more than 80% of ions into the  $S_{1/2}^{M_j=+1/2}$  state.

(C) Search. The density of tagged particles at a chosen search position  $n_t(r_s, t)$  is measured nondestructively with a perpendicular beam tuned to the peak of the “cyclone” transition  $S_{1/2}^{M_j=+1/2} \rightarrow P_{3/2}^{M_j=+3/2}$  which decays only to  $S_{1/2}^{M_j=+1/2}$ . This beam is weak and is on less than 10% of the time, to minimize “sideband” excitation of other transitions.

Each reset/tag/search cycle determines  $n_t(r_s, t)$  for  $0.05 < t < 100 \text{ s}$ , and repeating this cycle for 31 different  $r_s$  gives the test particle evolution  $n_t(r, t)$ . Figure 2(c) shows the normalized test particle profiles  $n_t(r)/n(r)$  at  $t = 0.05, 6, \text{ and } 15 \text{ s}$  for a case where the ions were tagged at  $r_t = 0.5 \text{ cm}$ . Visually, the tagged particles appear to diffuse radially towards the equilibrium state of  $n_t/n = \text{const}$ .

The test particle flux  $\Gamma_t$  can be obtained from these data as

$$\Gamma_t(r, t) = -\frac{1}{r} \int_0^r dx x \frac{\partial}{\partial t} n_t(x, t) + \int_0^r dx x \frac{2n_t(x, t) - n(x)}{\tau_s(x)}. \quad (1)$$

The second term corrects for the slow spontaneous spin flips at the separately measured rate  $\tau_s^{-1}$ . With this correction, the total number of tagged particles is conserved to within 10%. This flux is then compared to a transport model including both local diffusion coefficient  $D(r)$  and convective velocity  $V(r)$ :

$$\Gamma_t(r, t) = -D(r) n(r) \frac{\partial}{\partial r} \frac{n_t(r, t)}{n(r)} + V(r) n_t(r, t). \quad (2)$$

Figure 3 shows the measured normalized flux  $\Gamma_t/n_t$  versus the measured normalized gradient:  $(n/n_t)(\partial/\partial r)(n_t/n)$  for one particular radius  $r_s = 0.318$  cm. The different points represent different times in the evolution. The straight line fit to the data gives  $D(r_s) = 3.3 \times 10^{-3}$  cm<sup>2</sup>/sec and  $V(r_s) = -1.4 \times 10^{-4}$  cm/s. We expect and obtain  $V(r) = 0$  to experimental accuracy, since these test particles are transported exactly the same as all other ions, and the total density  $n(r)$  is independent of time. Similarly, with  $n_t/n \equiv \beta g(r)$ , Eq. (2) shows that  $\Gamma_t/n_t$  depends only on the profile  $g(r)$  but not the absolute magnitude  $\beta$ ; therefore Eq. (2) is valid even for  $n_t/n = O(1)$ . Figure 3 shows normalized flux proportional to normalized gradient over a range of 20 (Fick's law), indicating that higher powers of the gradient are not important here.

Figure 4 shows the measured diffusion coefficients  $D$  for densities  $1 \times 10^6$  cm<sup>-3</sup>  $< n < 4 \times 10^7$  cm<sup>-3</sup> (from different  $r_s$  and from different plasmas), for  $0.05 < T < 3$  eV (from auxiliary heating), and for magnetic fields  $0.8 < B < 4$  T. The diffusion coefficients are normalized by  $n_q B^{-2} \ln(\lambda_D/r_c)$  for comparison to classical and  $\mathbf{E} \times \mathbf{B}$  drift collisional theories described below; this normalization indicates that our data are consistent with  $B^{-2}$  scaling over a range of 5 in magnetic field as discussed below. Over a wide range of temperatures, the data are about ten times greater than expected from classical collisions alone ( $D_{ii}^{\text{class}}$  shown by solid lines). This enhanced diffusion does not seem to be caused by the rotating wall, which keeps the ion cloud in steady state: The open symbols of Fig. 4 were obtained with the rotating wall signal turned off during the test particle evolution.

Classical transport theory describes steps in the position of an ion guiding center due to collisional scattering of the ion velocity vector, arising from binary ion-ion

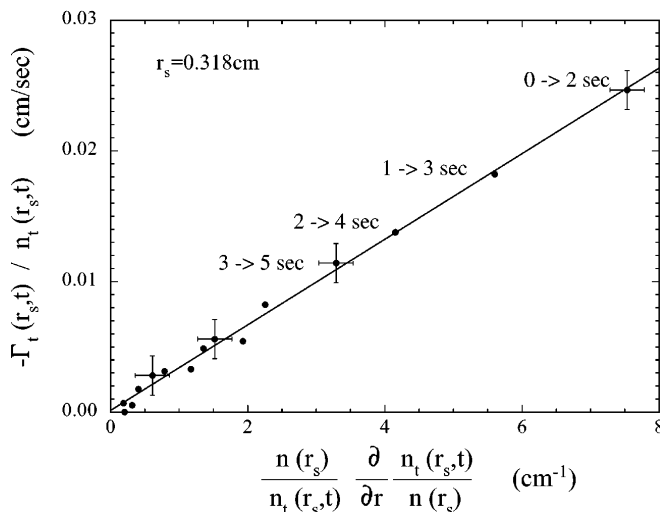


FIG. 3. Measured normalized test particle flux  $\Gamma_t/n_t$  versus normalized test particle gradient, showing Fick's law of diffusion, for the evolution of Fig. 2(c).

collisions with impact parameters  $b < \rho < r_c$ . Here  $b \equiv e^2/T = (1.44 \text{ nm})T^{-1}$  is the classical distance of closest approach, and  $r_c \equiv \bar{v}/\Omega_c = (500 \mu\text{m})T^{1/2}B^{-1}$  is the cyclotron orbit radius. The predicted diffusion coefficient is [1]

$$D_{ii}^{\text{class}} = \frac{5}{4} \left( \frac{16\sqrt{\pi}}{15} n b^2 \bar{v} \ln \Lambda \right) r_c^2 \equiv \frac{5}{4} \nu_{ii} r_c^2. \quad (3)$$

Here  $\nu_{ii} \approx (0.10 \text{ s}^{-1})T^{-3/2}(n/10^6)$  is the ion-ion momentum-transfer collision rate, with Coulomb logarithm  $\ln \Lambda = \ln(r_c/b)$  for a magnetized plasma [12], giving  $D_{ii}^{\text{class}} \approx (3.1 \times 10^{-4} \text{ cm}^2/\text{s})T^{-1/2}B^{-2}(n/10^6)$ . The range of  $[n_q \ln(\lambda_D/r_c)]^{-1} B^2 D_{ii}^{\text{class}}$  is shown by the solid curves in Fig. 4; the range arises from the  $\ln(\lambda_D/r_c)$  normalization which is not in classical theory. Of course, classical ion velocity scatterings from ion-neutral collisions can also give ion diffusion, but this coefficient  $D_{iN} \approx \nu_{iN} r_c^2 \approx (2.4 \times 10^{-4} \text{ cm}^2/\text{s})(T^{1/2} + 0.5)T B^{-2}$  is negligible at low pressure and temperature (dotted line). Also,  $D_{iN}$  does not depend on the ion density and has very different temperature scaling.

This enhanced test particle diffusion is observed even though measurements of velocity-space isotropization in these plasmas agree closely with classical theory. We have induced anisotropies between  $T_{\parallel}$  and  $T_{\perp}$ , and measured the relaxation of  $T_{\parallel}(t)$  and  $T_{\perp}(t)$  to a common final temperature  $T$ . Collisional theory predicts  $(d/dt)(T_{\perp} - T) = -\nu_{\perp 0}(T_{\perp} - T)$ , with relaxation rate  $\nu_{\perp 0} = 1.5\nu_{ii}$ . Figure 5 shows the measured velocity scattering rates  $\nu_{\perp 0}$  and the Fokker-Planck prediction [11], with no adjustable parameters. Thus, there are no anomalously large velocity-scattering collisions causing the enhanced test-particle diffusion. Note, however, that these collisions will keep the test particle distribution Maxwellian at temperature  $T$  during the transport.

Long-range " $\mathbf{E} \times \mathbf{B}$  drift" collisions [2,3] with impact parameters in the range  $r_c < \rho < \lambda_D$  are the likely explanation for the enhanced test particle diffusion. Two

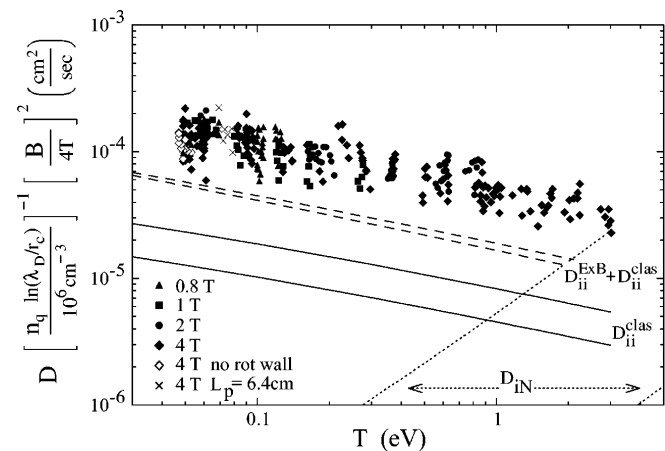


FIG. 4. Measured test particle diffusion coefficients  $D$  normalized to  $n_q B^{-2} \ln(\lambda_D/r_c)$  versus temperature. Theory curves show classical diffusion  $D_{ii}^{\text{class}}$  and estimates of  $\mathbf{E} \times \mathbf{B}$  drift diffusion  $D_{ii}^{\mathbf{E} \times \mathbf{B}}$  for the range of densities observed.

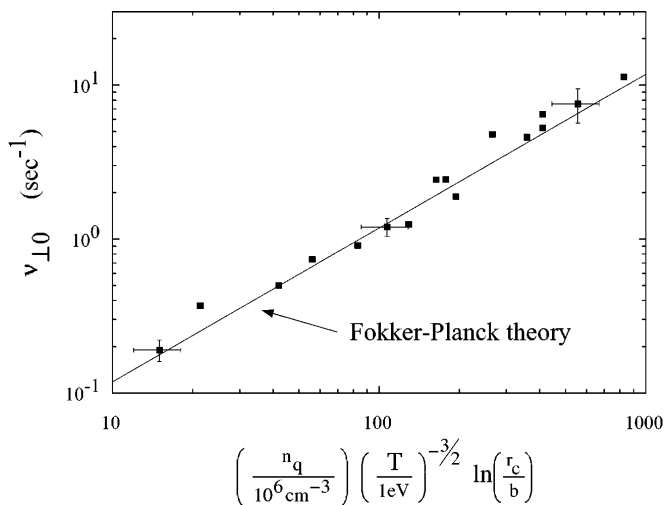


FIG. 5. Measured velocity-space isotropization rate  $\nu_{\perp 0}$  compared to the prediction of theory, with no adjustable parameters.

ions on field lines separated by  $\Delta r \lesssim \lambda_D$  with small relative axial velocity will interact for a long time, and will  $\mathbf{E} \times \mathbf{B}$  drift due to their mutual interaction field, even though there is no significant scattering of the velocity vectors. A simple estimate of the drifts evaluated on unperturbed orbits gives a diffusion coefficient

$$D_{ii}^{\mathbf{E} \times \mathbf{B}} = 2\sqrt{\pi} n b^2 \bar{v} r_c^2 \ln\left(\frac{\lambda_D}{r_c}\right) \ln\left(\frac{\bar{v}}{\Delta v_z}\right). \quad (4)$$

The minimum  $\Delta v_z$  that can be sustained by two ions is limited by velocity-scattering collisions and by rotational shear [3]. Diffusion of  $v_z$  from small-angle scatterings gives  $(\Delta v_z)^2 = \nu_{ii} \bar{v}^2 \tau$ , and the interaction time  $\tau$  is set by  $(\Delta v_z)\tau = \lambda_D$ , giving  $\bar{v}/\Delta v_z = (\omega_p/\nu_{ii})^{1/3}$ . Alternately, shear in the cross-field drift motion of ions separated by  $\lambda_D$  may limit the interaction time, giving  $\bar{v}/\Delta v_z \approx (2\lambda_D/r_c) |f_E/r (\partial/\partial r)f_E|$ .

An estimate for  $D_{ii}^{\mathbf{E} \times \mathbf{B}} + D_{ii}^{\text{class}}$  with  $\Delta v_z$  limited by collisions is shown by the two dashed lines on Fig. 4. Since the density enters as  $\ln(n^{-1/2})$ , it cannot be scaled out, and the two dashed curves represent the density extremes of the data, i.e.,  $n = 1 \times 10^6 \text{ cm}^{-3}$  and  $4 \times 10^7 \text{ cm}^{-3}$ . For these plasmas the shear limitation is generally negligible. The  $\times$ 's in Fig. 4 are for shorter plasmas, suggesting that end effects are not a dominant source of the discrepancy. To obtain the  $B$  scaling of the long-range transport, we fit all the data to  $D - D_{ii}^{\text{class}} = \alpha n_q T^{-1/2} \ln(\lambda_D/r_c) \ln(\bar{v}/\Delta v_z) B^\beta$  and obtain  $\beta = -1.9 \pm 0.1$  and  $\alpha = (1.0 \pm 0.2) \times 10^{-4}$ , whereas Eq. (4) would give  $\beta = -2$  and  $\alpha = 3.67 \times 10^{-5}$ .

For test particle transport, we observed ten times greater diffusion than predicted by classical theory, but still scaling as  $B^{-2}$ , neglecting factors of order  $\ln(B)$ . Estimates of  $\mathbf{E} \times \mathbf{B}$  drift collisions give a factor of 3 enhancement, but the evaluation along unperturbed orbits is questionable, and the theory is still being developed. In contrast, theory

suggests that bulk viscous transport is greatly enhanced by these long-range interactions: Viscosity can be orders of magnitude larger than expected from Boltzmann theory, scaling as  $B^{-2}$  [3] or  $B^{-1}$  [19] rather than as  $B^{-4}$  [20]. The interpretation of enhanced viscosity in pure electron plasmas scaling as  $B^{-1}$  [9] as due to long-range interactions is in support of the present data being due to long range  $\mathbf{E} \times \mathbf{B}$  drift collisions. Further, there may be significant cross-field heat transport from these long-range interactions, analogous to that from waves [21].

This work was supported by Office of Naval Research Grant No. N00014-96-1-0239 and National Science Foundation Grant No. PHY94-21318. One of us (F. A.) thanks Dr. J. C. Bergquist for advice on laser frequency doubling. The technical support of R. Bongard is acknowledged.

\*Present address: National Institute of Standards and Technology, 325 Broadway, Boulder, CO 80303.

- [1] C. L. Longmire and M. N. Rosenbluth, *Phys. Rev.* **103**, 507 (1956).
- [2] E. M. Lifshitz, and L. P. Pitaevski, *Physical Kinetics* (Pergamon Press, New York, 1981), Sec. 60.
- [3] T. M. O'Neil, *Phys. Rev. Lett.* **55**, 943 (1985).
- [4] R. A. Stern, D. N. Hill, and N. Rynn, *Phys. Lett. A* **93**, 127 (1983).
- [5] R. McWilliams and M. Okubo, *Phys. Fluids* **30**, 2849 (1987).
- [6] A. F. Fasoli, F. N. Skiff, T. N. Good, and P. J. Paris, *Phys. Rev. Lett.* **68**, 2925 (1992).
- [7] F. N. Skiff and A. F. Fasoli, *Phys. Lett. A* **184**, 104 (1993).
- [8] P. C. Efthimion *et al.*, *Phys. Rev. Lett.* **75**, 85 (1995).
- [9] C. F. Driscoll, J. H. Malmberg, and K. S. Fine, *Phys. Rev. Lett.* **60**, 1290 (1988).
- [10] See, for example, *Non-Neutral Plasma Physics II*, edited by J. Fajans and D. Dubin, AIP Conf. Proc. No. 331 (AIP, New York, 1995).
- [11] A. Hyatt, C. F. Driscoll, and J. H. Malmberg, *Phys. Rev. Lett.* **59**, 2975 (1987); S. Ichimaru and M. N. Rosenbluth, *Phys. Fluids* **13**, 2778 (1970).
- [12] D. Montgomery, G. Joyce, and L. Turner, *Phys. Fluids* **17**, 2201 (1974).
- [13] F. Anderegg, X.-P. Huang, E. Sarid, and C. F. Driscoll, *Rev. Sci. Instrum.* (to be published).
- [14] R. A. MacGill, I. G. Brown, and J. E. Galvin, *Rev. Sci. Instrum.* **61**, 580 (1990).
- [15] X.-P. Huang, F. Anderegg, E. M. Hollmann, C. F. Driscoll, and T. M. O'Neil, *Phys. Rev. Lett.* **78**, 875 (1997).
- [16] J. C. Bergquist, H. Hemmati, and W. Itano, *Opt. Commun.* **43**, 437 (1982).
- [17] T. M. O'Neil, *Phys. Fluids* **24**, 1447 (1981).
- [18] F. Skiff, T. N. Good, F. Anderegg, and P. J. Paris, *Phys. Lett. A* **137**, 57 (1989).
- [19] D. H. E. Dubin and T. M. O'Neil, *Phys. Rev. Lett.* **60**, 1286 (1988).
- [20] T. M. O'Neil and C. F. Driscoll, *Phys. Fluids* **22**, 266 (1979).
- [21] M. N. Rosenbluth and C. S. Liu, *Phys. Fluids* **19**, 815 (1976).